

Wave propagation on irregular grids

M. Pohl, H. Igel and F. Wenzel¹

keywords: *pseudospectral methods, irregular grids*

ABSTRACT

By solving the wave equation on regular or irregular grids wave propagation can be studied in any complex model 2D and 3D. However, the model complexity is limited by the computer capacity. Pseudospectral methods have the advantage of being exact in terms of spatial derivatives and therefor require less grid points per wavelength than finite difference methods. Models with curved layer boundaries, however, require a dense grid spacing to avoid diffraction. By introducing curved grids with layer boundaries aligned to the grid, this problem can be solved.

INTRODUCTION

Pseudospectral methods are useful tools for solving the wave equation on 2D and 3D grids. Since the spatial derivatives are exact one can choose a coarser grid and therefore larger time steps. Thus, one can speed up numerical simulation runs by several times (Fornberg, 1987). Furthermore, no dispersion effects due to discretisation errors occur. Interfaces not aligned with the grid, however, lead to other undesired effects. The corners in the discretisation of a layer boundary not aligned with the grid act as diffractors. To avoid this unphysical noise the grid spacing must be reduced. In such cases the advantages of a coarser grid using pseudospectral methods can not be used. We introduce a simple mapping scheme to a Chebyshev code and align the layer boundaries with the grid. Similar schemes were applied by Fornberg (1988) and Tessmer and Kosloff (1993).

METHOD

Our code is based on the Chebyshev Collocation method (Augenbaum, 1990; Carcione and Wang, 1993). The solution of the wave equation is expanded in terms of Cheby-

¹**email:** Melanie.Pohl@phys.uni-karlsruhe.de

shev polynomials. In the computational domain the grid is defined by the Gauss–Lobatto collocation points. Since this grid becomes very fine near the grid boundaries, a one–dimensional stretching function is applied for each coordinate in order to increase the time steps for the integration. For the forward integration in time we use a fourth order Runge–Kutta scheme. Absorbing boundary conditions are imposed by a characteristic treatment.

Layer topography is introduced by mapping the stretched rectangular grid onto a curved grid. All formulae are written for the 3D case. The physical curved grid has the coordinates X , Y and Z . The mapping functions are

$$\begin{aligned} X(x, y, z) &= x \\ Y(x, y, z) &= y \\ Z(x, y, z) &= z + g(x, y, z) \end{aligned}$$

with the topography function $g(x, y, z)$. In our case we require g to be a continuous differentiable function. By the mapping only the z –coordinates are altered. Additionally, the topography function is tapered by a sinus function in z to obtain flat boundaries.

For the velocity–stress formulation we then yield:

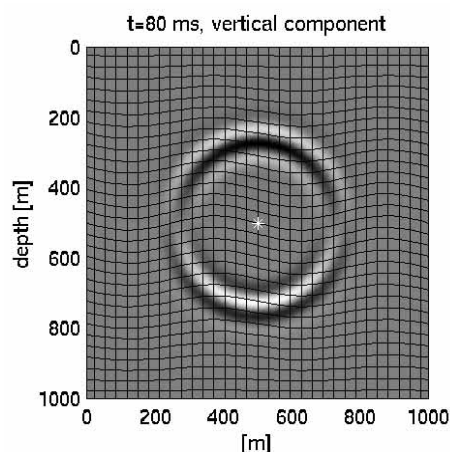
$$\begin{aligned} \rho \dot{v}_X &= \frac{\partial \sigma_{XX}}{\partial x} + \frac{\partial \sigma_{XX}}{\partial z} c_x + \frac{\partial \sigma_{XY}}{\partial y} + \frac{\partial \sigma_{XY}}{\partial z} c_y + \frac{\partial \sigma_{XZ}}{\partial z} c_z \\ \rho \dot{v}_Y &= \frac{\partial \sigma_{XY}}{\partial x} + \frac{\partial \sigma_{XY}}{\partial z} c_x + \frac{\partial \sigma_{YY}}{\partial y} + \frac{\partial \sigma_{YY}}{\partial z} c_y + \frac{\partial \sigma_{YZ}}{\partial z} c_z \\ \rho \dot{v}_Z &= \frac{\partial \sigma_{XZ}}{\partial x} + \frac{\partial \sigma_{XZ}}{\partial z} c_x + \frac{\partial \sigma_{YZ}}{\partial y} + \frac{\partial \sigma_{YZ}}{\partial z} c_y + \frac{\partial \sigma_{ZZ}}{\partial z} c_z \\ \dot{\sigma}_{XX} &= \lambda \left(\frac{\partial \dot{v}_X}{\partial x} + \frac{\partial \dot{v}_X}{\partial z} c_x + \frac{\partial \dot{v}_Y}{\partial y} + \frac{\partial \dot{v}_Y}{\partial z} c_y + \frac{\partial \dot{v}_Z}{\partial z} c_z \right) + 2\mu \left(\frac{\partial \dot{v}_X}{\partial x} + \frac{\partial \dot{v}_X}{\partial z} c_x \right) \\ \dot{\sigma}_{YY} &= \lambda \left(\frac{\partial \dot{v}_X}{\partial x} + \frac{\partial \dot{v}_X}{\partial z} c_x + \frac{\partial \dot{v}_Y}{\partial y} + \frac{\partial \dot{v}_Y}{\partial z} c_y + \frac{\partial \dot{v}_Z}{\partial z} c_z \right) + 2\mu \left(\frac{\partial \dot{v}_Y}{\partial y} + \frac{\partial \dot{v}_Y}{\partial z} c_y \right) \\ \dot{\sigma}_{ZZ} &= \lambda \left(\frac{\partial \dot{v}_X}{\partial x} + \frac{\partial \dot{v}_X}{\partial z} c_x + \frac{\partial \dot{v}_Y}{\partial y} + \frac{\partial \dot{v}_Y}{\partial z} c_y + \frac{\partial \dot{v}_Z}{\partial z} c_z \right) + 2\mu \left(\frac{\partial \dot{v}_Z}{\partial z} c_z \right) \\ \dot{\sigma}_{XY} &= \mu \left(\frac{\partial \dot{v}_X}{\partial y} + \frac{\partial \dot{v}_X}{\partial z} c_y + \frac{\partial \dot{v}_Y}{\partial x} + \frac{\partial \dot{v}_Y}{\partial z} c_x \right) \\ \dot{\sigma}_{XZ} &= \mu \left(\frac{\partial \dot{v}_X}{\partial z} c_z + \frac{\partial \dot{v}_Z}{\partial x} + \frac{\partial \dot{v}_Z}{\partial z} c_x \right) \\ \dot{\sigma}_{YZ} &= \mu \left(\frac{\partial \dot{v}_Y}{\partial z} c_z + \frac{\partial \dot{v}_Z}{\partial y} + \frac{\partial \dot{v}_Z}{\partial z} c_y \right) \end{aligned}$$

where λ and μ are the Lamé parameters and ρ is the density. The terms c_x , c_y and c_z denote products of derivatives of the topography function.

EXAMPLES IN 2D

In order to test the accuracy we chose a homogeneous model ($1000 \times 1000\text{m}$, 161×161 grid points) and located the explosive source in the center of the model volume. As topography function we used a sinus function with an amplitude of 20m and a wavelength of 500m . Figure 1 shows the wavefront after 80ms .

Figure 1: Wavefront after 80ms . Every 5th gridline is displayed. The wavefront is not altered by the transformed grid. The star marks the source location.



Another example studies the effect of layer topography up to subwavelength scale onto the reflection amplitudes. Here, we chose a layer boundary with a syncline directly underneath the source. The halfwidth of the syncline varies from 4λ to 0.5λ with λ being the dominant wavelength of the source signal. For all four models we used the same number of grid points. In order to avoid interference with the direct wave, source and receivers are situated at the same depth. All boundaries are absorbing. Figure 2 and 3 show the corresponding snapshots and seismograms.

CONCLUSION

This technique enables us to simulate wave propagation in 2D and 3D in acceptable time. It can be used to study the reflection properties of media with laterally varying layer boundaries. The technique can be extended to include arbitrarily shaped topography functions, e.g. by using spline functions.

REFERENCES

Augenbaum, J. M., 1990, The pseudospectral method for limited-area elastic wave calculations;, 1–14.

- Carcione, J. M., and Wang, J.-P., 1993, A Chebyshev collocation method for the elastodynamic equation in generalized coordinates: *Comp. Fluid Dynam. J.*, **2**, no. 3, 269–290.
- Fornberg, B., 1987, The pseudospectral method: Comparison with finite differences for the elastic wave equation: *Geophysics*, **52**, no. 4, 483–501.
- Fornberg, B., 1988, The pseudospectral method: Accurate representation of interfaces in elastic wave calculations: *Geophysics*, **53**, no. 5, 625–637.
- Tessmer, E., and Kosloff, D., 1993, 3–D elastic modelling with surface topography by a Chebyshev spectral method: *Geophysics*, **59**, no. 3, 464–473.

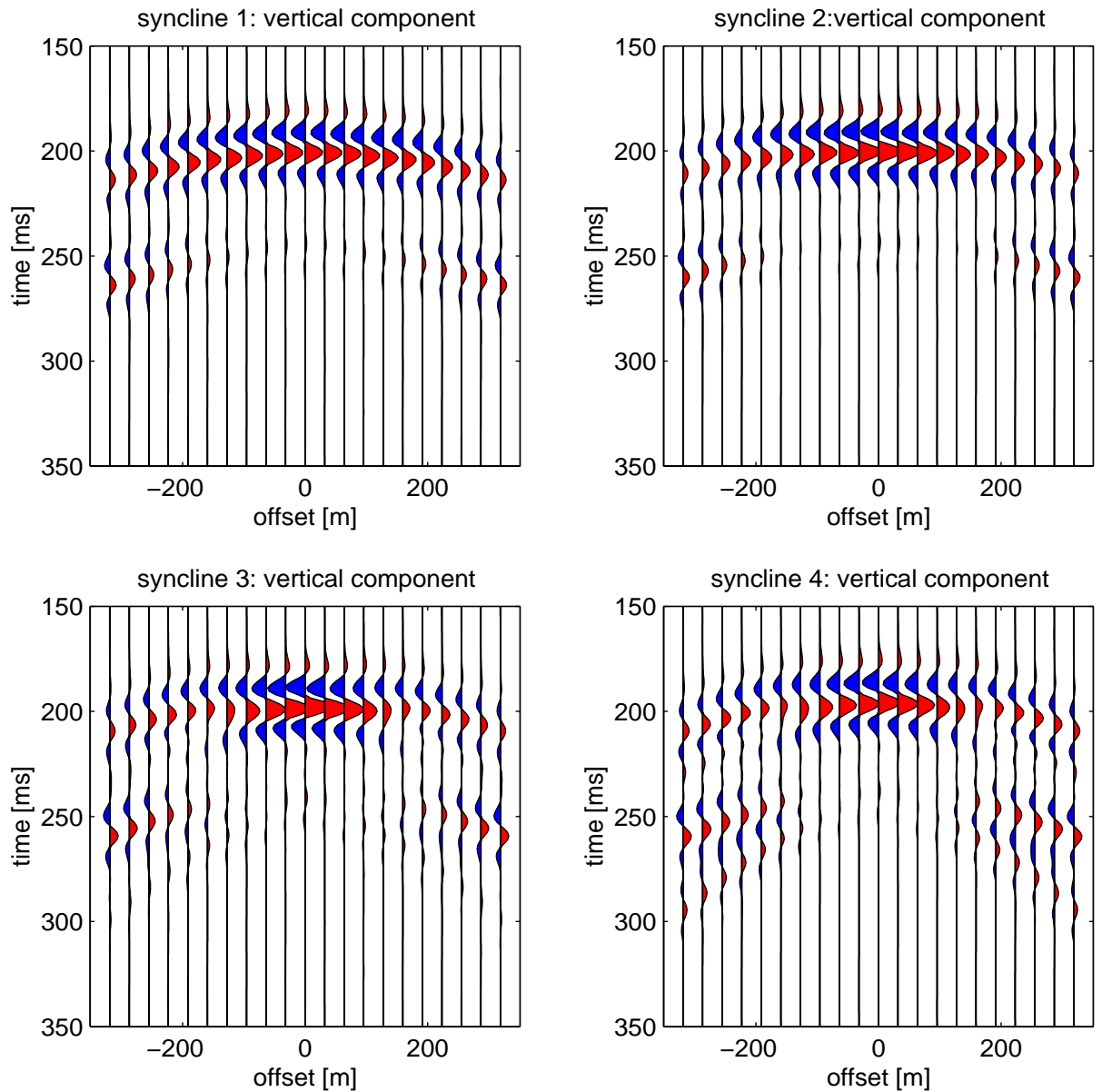


Figure 3: Seismograms corresponding to figure 2. The amplitudes are normalized to the maximum of all plots. The first arrival is the reflected p-wave followed by the p-to-s conversion. The focussing effect is strongest for syncline 3.